Available online at www.sciencedirect.com

ScienceDirect

Energy Procedia 94 (2016) 443 – 451

Energy Procedia

13th Deep Sea Offshore Wind R&D Conference, EERA DeepWind'2016, 20-22 January 2016, Trondheim, Norway

Numerical and experimental investigation of breaking wave interaction with a vertical slender cylinder

Mayilvahanan Alagan Chella[a,*], Xavier Ros Collados[c], Hans Bihs[a], Dag Myrhaug[b], Øivind Asgeir Arntsen[a]

[a]*Department of Civil and Engineering, Norwegian University of Science and Technology,NO-7491 Trondheim, Norway*
[b]*Department of Marine Technology, Norwegian University of Science and Technology,NO-7491 Trondheim, Norway*
[c]*DNV GL Offshore Technology, Trondheim, Norway*

Abstract

Offshore wind turbine substructures consisting of cylindrical members are exposed to highly non-linear and breaking waves in shallow waters [1]. Those structures experience extreme impulsive loads of short duration from breaking waves that can cause permanent structural damage[2]. The main purpose of the present paper is to investigate the wave impact forces on a slender cylinder from plunging breaking waves in shallow waters both experimentally and numerically. The present study consists of two major parts: laboratory measurements and numerical simulations. The laboratory experiments are performed with regular waves. Plunging breaking waves are generated and free surface elevations are measured around the cylinder. Next, numerical simulations are carried out in the three-dimensional numerical wave tank REEF3D. The model is based on the incompressible Reynolds-averaged Navier-Stokes equations together with the $k-\omega$ for turbulence and the level set method for free surface. The numerical results are compared with the laboratory measurements in order to validate the numerical model. A good agreement between the computed results and the experimental data is seen for the breaking wave properties. Further, the breaking wave forces and the free surface deformations during the interaction of plunging breaking waves with a vertical cylinder are investigated and they are reasonably well represented in the numerical simulations.

Peer-review under responsibility of SINTEF Energi AS

Keywords: Breaking waves; breaking wave forces; breaking wave interaction; numerical modelling; free surface deformations

1. Introduction

Offshore wind energy is gaining spotlight as a potentially huge, clean and renewable energy source. Currently, most of the offshore wind farms have been developed in shallow waters of depths between 5 to 30m. Offshore wind turbine (OWT) substructures consisting of cylindrical members are exposed to highly non-linear and breaking waves in shallow waters [1]. Wave impacts exert high intensive loads on structures and the load durations are shorter or

*Corresponding author. Tel.: +0-000-000-0000 ; fax: +0-000-000-0000.
E-mail address: acm@ntnu.no

Peer-review under responsibility of SINTEF Energi AS
doi:10.1016/j.egypro.2016.09.214

comparable with the natural period of the structures. In particular, a shorter rise time wave impact event can cause more intense impact force on a structure. Moreover, the forces from breaking waves are the largest and exert the most severe loads, causing permanent structural damage to structural members. In some cases, this loading condition governs the design of the OWT substructures[1]. Monopile is the most common foundation type for offshore wind turbines in shallow waters [3]. In addition, hydrodynamic loads from highly nonlinear shallow water waves have a significant influence on the fatigue life of OWT [4]. Specifically, understanding the physical processes during the wave breaking has always been a key factor in the estimation of hydrodynamic loads on OWT substructures.

Wave breaking is a natural process involving transformation of wave energy into turbulent energy leading to a rapid transition of the free surface, that exerts massive hydrodynamic loads on marine structures [5]. A wave undergoes deformation, i.e. the wave height and local wave steepness increase as it propagates over decreasing water depth, leading to an increase in the forward momentum. Further, the slope of the wave front and the crest particle velocity increases continuously until the wave breaks. When the breaking wave interacts with a vertical cylinder, a rapid change in the forward momentum occurs, causing an impact force on it in a very short duration [6]. The shape of the wave profile and the wave celerity at breaking are important considerations for describing the wave impact force. Numerous studies have investigated the nonlinear hydrodynamic loads from breaking waves on offshore structures in deep waters (e.g. [7,8]).

Several experimental studies have been carried out to investigate the interaction between breaking waves and a vertical cylinder (e.g. [6,9–12]). The studies also show that the application of the Morison equation [13] to estimate the breaking wave force on a fixed vertical cylinder is not straight forward, but the equation can be used to predict the total breaking wave force by including a separate impact force term. However, the inputs concerning the wave shape and the breaking wave celerity need to be known in order to determine the theoretical total force from breaking waves [6,9,11]. Numerical modelling of of breaking waves and the interaction with OWT substructures are subjected to significant uncertainties since the underlying physical processes are still not fully understood. The evolution of breaking waves and their interaction with structures can be modelled numerically with computational fluid dynamics (CFD) models based on the Navier-Stokes equations. A number of numerical investigations have been attempted to model breaking waves and the associated flow characteristics in shallow waters (e.g. [14–19]). A few numerical studies have been carried out to investigate the interaction between breaking waves and structures [3,20,21]. Although these investigations reported many interesting results, little work has examined the characteristics of breaking wave forces and the resulting free surface flow features around a structure.

The main purpose of the present paper is to investigate the interaction of plunging breaking waves with a vertical slender cylinder in shallow waters both experimentally and numerically. The present study consists of two major parts: laboratory measurements and numerical simulations. First, the laboratory experiments are performed with regular waves in a 33m long glass wave flume. Plunging breaking waves are generated and free surface elevations along the wave tank and the wave impact forces are measured. Next, numerical simulations are conducted in the three-dimensional numerical wave tank REEF3D [17,22]. The numerical model is based on the incompressible Reynolds-averaged Navier-Stokes equations together with the $k - \omega$ for turbulence and the level set method for the free surface. The numerical results are compared with the laboratory measurements in order to validate the numerical model. A good agreement between the computed results and the experimental data is seen for the characteristics of breaking waves and the wave celerity at breaking. Further, the numerical study examines the wave celerity at breaking, the pressure distribution, and the free surface deformations during the interaction of breaking waves with a cylinder. In addition, the breaking wave forces for waves with different frequencies are also presented and discussed.

2. Numerical model

In the present study, the open source CFD model REEF3D has been used to simulate breaking waves and their interaction with a slender cylinder. The present numerical model has been thoroughly validated and tested for several hydrodynamic problems such as waves breaking over slopes [17,19], waves breaking over an impermeable slope [18] and non-breaking wave forces on vertical cylinders [22,23]. The model has also been validated for modeling breaking wave forces [24,25] and utilized to investigate the breaking forces on slender vertical cylinders under different wave impact scenarios and the flow features around them. The present numerical model uses higher-order numerical schemes in order to achieve good numerical accuracy and stability. The governing equations of the model are the

incompressible RANS equations and the continuity equation.

$$\frac{\partial u_i}{\partial x_i} = 0 \tag{1}$$

$$\frac{\partial u_i}{\partial t} + u_j \frac{\partial u_i}{\partial x_j} = -\frac{1}{\rho}\frac{\partial p}{\partial x_i} + \frac{\partial}{\partial x_j}\left[(\nu + \nu_t)\left(\frac{\partial u_i}{\partial x_j} + \frac{\partial u_j}{\partial x_i}\right)\right] + g_i \tag{2}$$

Here, u is the velocity averaged over time t, ρ is the fluid density, p is the pressure, ν is the kinematic viscosity, ν_t is the eddy viscosity, and g is the acceleration due to gravity. The fifth-order weighted essentially non-oscillatory (WENO) scheme is employed for the convective descretization [26]. The third-order accurate TVD Runge-Kutta scheme is used for the time descretization [27]. The simulation time steps are controlled by an adaptive time-stepping method [28] which is based on the Courant-Friedrichs-Lewy (CFL) criterion. The CFL criterion is maintained and the simulation time step is adjusted for each iteration. The CFL number of the present numerical study is 0.1 and the simulations are performed at very small time steps that are fine enough to capture the nonlinear dynamic effects.
A strong coupling between the velocity and pressure fields is obtained by using the staggered grid arrangement. The free surface is computed using the level set method and it is defined as the zero level set of the signed distance function $\phi(\vec{x}, t)$ on the computational domain. The location and the sign of the zero level set function indicate the fluid phase. Theoretically, the VOF method is mass conservative, but due to either artificial interface compression schemes for an algebraic VOF method or interface reconstruction and propagation for a geometric VOF method, numerical errors are introduced. The level set method is not mass conservative, but due to differentiability high order discretization is possible, keeping mass errors at a minimum together with an advanced initialization scheme. In order to maintain the mass conservation property of the level set method during the free surface computations, an additional reinitialization scheme employed in the numerical model [29,30]. Turbulence under the breaking waves is described with the two equation $k - \omega$ model. The wave generation in the numerical wave tank is based on a relaxation method proposed by Larsen and Dancy [31] and Jacobsen et al. [32]. The wave absorption is employed using the active absorbing beach [33]. The total wave force on a vertical cylinder from breaking waves is computed based on the pressure p and the normal component of viscous stress tensor τ over the surface of the cylinder as follows:

$$F = \int_{\Omega} (-\mathbf{n}p + \mathbf{n}.\tau) d\Omega \tag{3}$$

where $\mathbf{n}$ is the normal vector to the surface of the cylinder Ω. The static pressure component is caused by the water column in front of the cylinder. Though the static component is not significant in estimating the impact force, it plays an important role in describing the total force from breaking waves. The theoretical description of total force from breaking waves does not account for the static pressure component [9]. In the present numerical simulations, the total force is calculated by integrating the total pressure around the cylinder including the static pressure component. A three-dimensional ghost cell immersed boundary method (GCIBM) [34] is employed to represent the solid boundaries. The numerical model is fully parallelised and the present simulations are performed on NOTUR supercomputer Vilje on a large number of processors [35]. Detailed information on the numerical model can be found in [17,19,22].

3. Results and Discussions

3.1. Experimental set-up

All the experiments have been carried out at carried out in the wave flume Sjøfrid at the SINTEF Technology and Society, Coast and Harbour Research Laboratory in Trondheim. The wave flume is 33 m long and it has a width of 1 m. The experimental test set-up is shown in Fig. 1. The deep water part close to the wave generation zone has a water depth of 0.90m. The shallow water part starts at a distance of 11.2 m from the paddle and has four different slopes. The first one, of approximately 1:9 slope, has a horizontal length of 5 m. The second slope decreases to an approximately 1:50 slope for a horizontal length of 1.85 m. It is followed by a horizontal zone with a length of 2.5 m. Finally, a downward slope of approximately 1:3.7 for a 2.2 m horizontal length. The cylinder of diameter D=0.06m is placed on the second slope, at 16.95 m distance from the wave paddle (Fig. 1). The bottom end of the cylinder is fixed

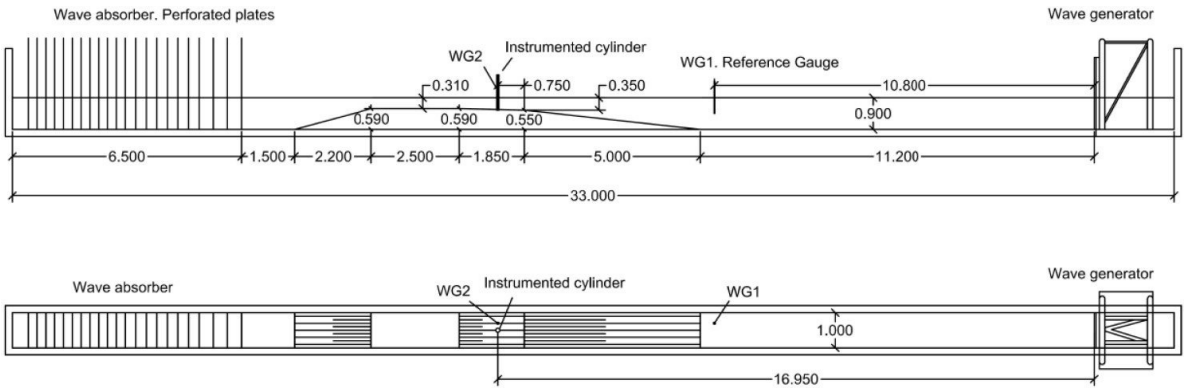

Fig. 1. Experimental set-up

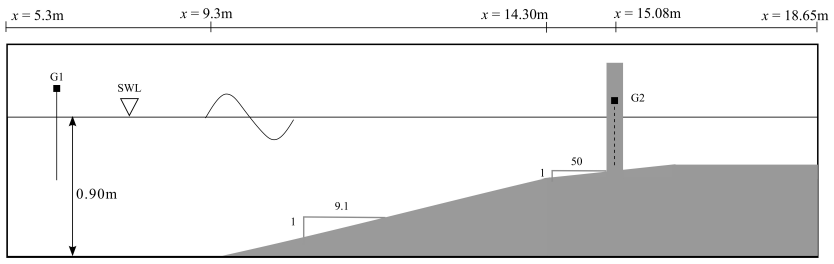

Fig. 2. Computational domain

to a base plate at the channel bottom and the top end is fixed to two orthogonal steel beams clamped to the channel walls. During the tests, waves are measured at two locations: WG1 and WG2 (Fig. 1). The sampling frequency of all response and wave data is set to 20 kHz. Three experimental cases with regular waves with frequencies around 0.5 Hz are considered in the present study (Table 1).

Table 1. Experimental cases.

Case	Wave frequency, f (Hz)	Wave period, T (s)	Deep water wave height, H_0 (m)
1	0.48	2.08	0.219
2	0.51	1.96	0.240
3	0.54	1.86	0.226

3.2. Numerical set-up

The numerical model for simulating the interaction of breaking waves is validated with the experimental data. In order to improve the computational efficiency, some changes have been made carefully to the computational set-up without effecting the quality and characteristics of waves. In the numerical simulation, the 12m long flat bed portion is reduced to 5m and the numerical beach with active absorption is introduced at the end of the submerged rectangular part behind the cylinder as shown in Fig. 2. The size of the numerical wave tank is L_x=18.65m, L_y=0.30m, and L_z=1.60m and it is descretized into 8.40 million uniform cells with a grid size dx=0.01m. The free surface elevation and the kinematics are defined in the wave generation zone using the fifth-order Stokes wave theory [36]. In order to test the dependency of numerical results on the grid size, the simulations are carried out for three different grid sizes (dx=0.05m, 0.025m and 0.01m). The simulation case with the maximum wave steepness (case 3, Table 1) is considered for the grid refinement study. Table 2 presents the computed wave height (H_b) and the wave surface

elevation (η_b) at breaking. The simulated results for the finest grid size (dx=0.01m) match well with the experimental

Table 2. Grid refinement study (case 3).

Grid size, dx (m)	H_b (m)	η_b (m)	C_b (m/s)
Experiments	0.246	0.175	2.20
0.010	0.249	0.182	2.240
0.025	0.213	0.155	2.212
0.050	0.196	0.143	2.185

results for the wave height, wave surface elevation, and wave celerity at breaking. Moreover, the numerical results for dx=0.025m and 0.05m are lower than the measured values. Therefore, the grid size of dx=0.01m is selected for the simulations.

3.3. Simulation of breaking waves over slopes

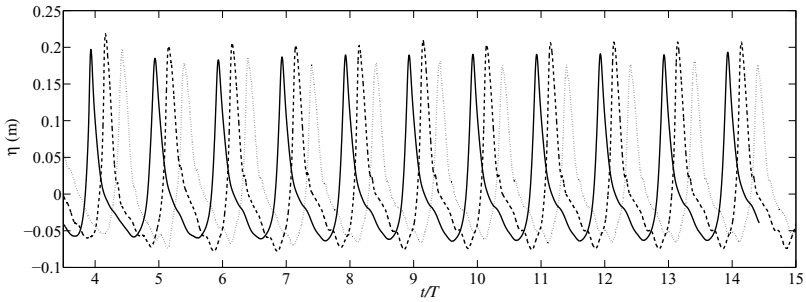

Fig. 3. Simulated water surface elevations in front of the cylinder versus normalized time (t/T) for cases 1 (solid line), 2 (dashed line) and 3 (dotted line)

Fig. 3 shows the simulated water surface elevations (η) in front of the cylinder for cases 1, 2 and 3. The maximum and minimum water surface elevations appear for case 2 and case 3, respectively. For all three cases, the wave height increases and the wave profile shape becomes sharper as the waves propagate over the slope due to shoaling. As a result, a significant change in the incident wave characteristics (Table 3) and the wave profile shape occur. The comparison of simulated and measured results for the wave surface elevation (η_b) and wave height at breaking (H_b), the breaker depth index ($\gamma_b = H_b/d_b$), and the breaking wave celerity (C_b) are listed in Table 3. The simulated η_b and H_b are almost the same as the measured data (Table 3). This implies that the wave crest and the wave trough are accurately captured in the simulations. In addition, the simulated γ_b is consistent with the measured γ_b, showing that the numerical waves break at the same location as in the laboratory experiments farther up on the slope at shallower water depth. At the same time, the part of the wave crest travels faster than the rest of the wave as the particle velocity at the wave crest becomes larger than the wave celerity. Therefore, the prediction of the wave celerity at breaking is essential for estimating the breaking wave force accurately. The breaking wave celerity is evaluated for each case and the comparison shows a good agreement with the experimental data (Table 3). Overall, the simulated results are in excellent agreement with the experimentally measured data for the breaking wave characteristics.

3.4. Simulation of interaction between breaking waves and a vertical cylinder

The interaction of breaking waves with a vertical cylinder is investigated for three different cases (Table 1). In the laboratory experiments, the wave impact forces are measured at the top part of the cylinder above still water level, while the total wave force on the cylinder due to breaking waves is not measured. In the numerical simulations, the total wave

Table 3. Comparison between the experimental results and the numerical results for breaking waves

Cases	Experimental results				Numerical results (dx=0.01m)			
	η_b(m)	H_b(m)	H_b/d_b	C_b(m/s)	η_b(m)	H_b(m)	H_b/d_b	C_b(m/s)
Case 1	0.180	0.249	0.72	2.20	0.188	0.251	0.73	2.25
Case 2	0.195	0.264	0.76	2.30	0.206	0.276	0.80	2.33
Case 3	0.175	0.246	0.71	2.20	0.182	0.249	0.72	2.26
Case 4	0.175	0.246	0.71	2.20	0.182	0.249	0.72	2.26

force is computed based on the pressure distribution along the cylinder. The total pressure is evaluated in front of the cylinder at a few points by inserting the pressure probe points and they are located one grid size (dx=0.01m) away from the cylinder surface. Fig. 4 shows the simulated pressure above still water level in front of the cylinder at z=1.06m (a), 1.02m (b), and 0.95m (c) for case 3. It appears that the shape of the pressure curve becomes narrower and sharper as the distance from the still water level increases. When the wave crest hits the cylinder (above still water level), the contribution of dynamic component of the pressure to the wave impact is larger than the static component. Fig. 5 presents the breaking wave force on the cylinder versus normalized time (t/T) for cases 1, 2 and 3. The maximum and minimum wave forces occur for case 2 and case 3, respectively, and this is consistent with the results for the water surface elevations (Fig. 3). The peak force appears narrower and sharper for case 3, which has a longer incident wave in the simulation cases than for cases 1 and 3. It is possible that the wave impact force contribution to the total force increases as the wave height increases.

Further, the free surface flow characteristics during the interaction of breaking waves with the cylinder are investigated. Fig. 6 depicts the free surface changes with the velocity variation for different time frames for case 3. When the crest particle velocity exceeds the wave celerity, the upper part of the wave moves faster than the lower part of the wave. As a result, the wave crest overturns forward with high velocity at the tip of the wave crest (Figs. 6 (a) and (b)). Further, the breaking wave impacts the cylinder at the crest level, exerting the maximum force on the cylinder. The front part of the wave is separated as it interacts with the cylinder and this leads to a rise of the water level in front of the cylinder (Figs. 6 (c) and (d)). The separated wave fronts meet and collide with each other downstream in the shadow zone of the cylinder, causing a water jet with high velocity downstream (Figs. 6 (e) and (f)). It is also possible that the development of downstream water jet and its interaction with waves and structures would affect the hydrodynamics around the neighboring structures significantly. The simulated results show that the free surface deformations around the cylinder during the interaction between the breaking waves and a vertical cylinder are well captured in the numerical simulations.

4. Conclusions

In the present study, the interaction of breaking waves with a slender vertical circular cylinder is investigated experimentally and numerically. Experiments are carried out in a wave flume with plunging breaking waves. The wave surface elevations along the wave tank and the wave impact forces on the cylinder are measured. In the numerical investigation, the open-source CFD model REEF3D [17,22] has been utilized to model the interaction of breaking waves with a slender vertical cylinder. The incompressible Reynolds-Averaged Navier-Stokes (RANS) equations are solved together with the level set method (LSM) for the free surface and the $k-\omega$ model for the turbulence. The characteristics of breaking waves and their interaction with a vertical cylinder for three different wave frequencies are investigated. The performance of the numerical model is evaluated by comparing the numerical results with the measured data. The simulated results show a good agreement with the experimental measurements for the wave surface elevation (η_b) and wave height (H_b) at breaking, the breaker depth index ($\gamma_b = H_b/d_b$), and the breaking wave celerity (C_b). Further, the pressure variation under the wave crest at breaking, the breaking wave forces and the free surface flow features along the cylinder are presented and discussed. The simulated results show that the numerical model represents the most prominent free surface flow features such as the the formation of forward overturning water crest, the separation and reconnection of wave crests around the cylinder, and the development downstream side water

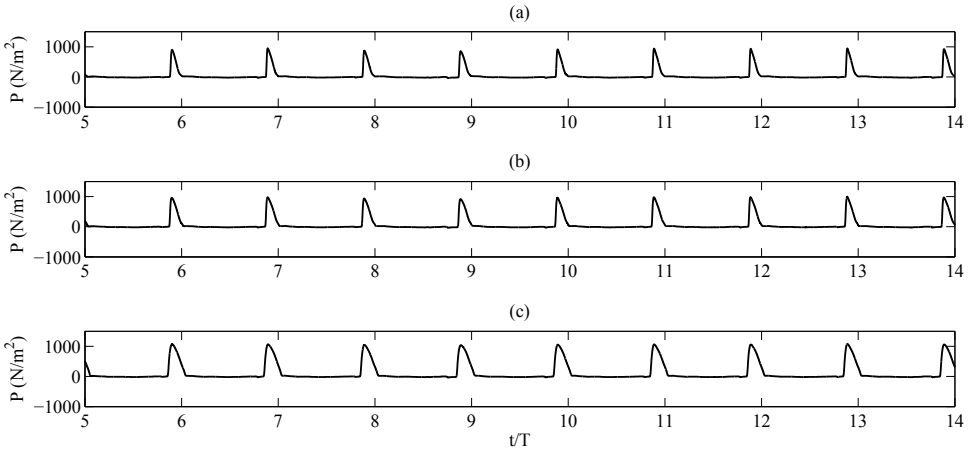

Fig. 4. Simulated pressure in front of the cylinder above still water level versus normalized time (t/T) at z=1.06m (a), 1.02m (b), and 0.95m (c) for case 3

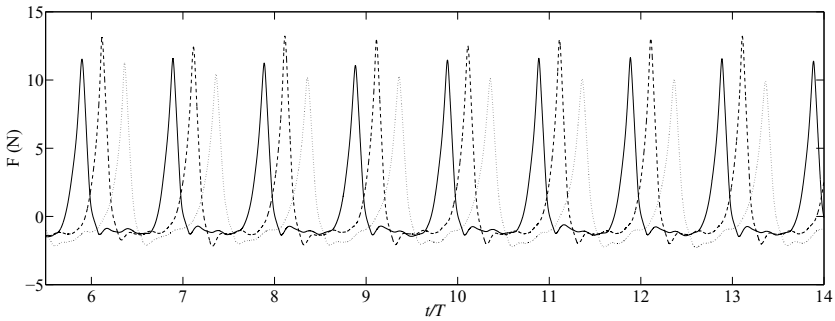

Fig. 5. Simulated breaking wave force on the cylinder versus normalized time (t/T) for cases 1 (solid line), 2 (dashed line) and 3 (dotted line)

jet. In the present investigation, the wave impact forces on the cylinder are measured in the laboratory experiments, but they are not modeled in the numerical simulations. Further, with finer grid resolutions, the detailed hydrodynamics around the cylinder and the resulting forces can be studied for different environmental conditions. In addition, the wave impact force on the cylinder can be calculated from the local pressure variation above the still water level in front of the cylinder. The wave run-up on the cylinder and the free surface flow features can also be investigated for different wave breaking conditions. This will enhance the current assessment of the breaking wave forces on marine structures and the free surface flow features around them.

Acknowledgements

The research work has been funded by the Research Council of Norway through the project "Hydrodynamic Loads on Offshore Wind Turbine Substructures due to Nonlinear Irregular Breaking, High Steep and Extreme Waves" (project number: 246810). The authors gratefully acknowledge the computing time granted by NOTUR (project number: NN2620).

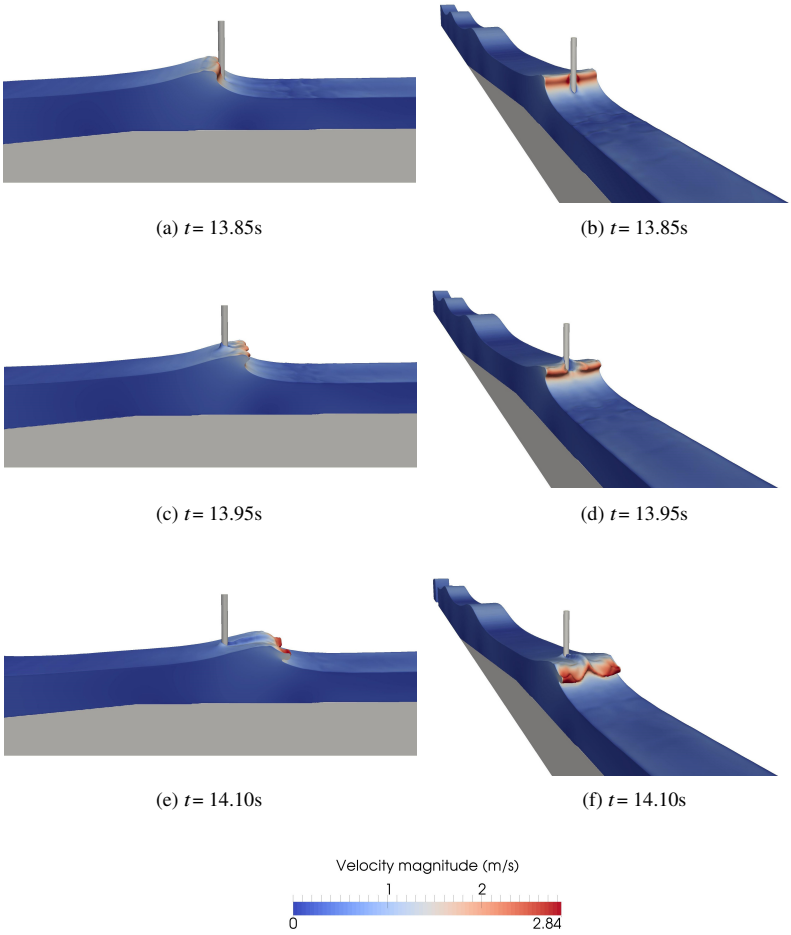

Fig. 6. Simulated free surface flow features with velocity magnitude (m/s) variation for different time instants for case 3

References

[1] Alagan Chella, M., Tørum, A., Myrhaug, D.. An overview of wave impact forces on offshore wind turbine substructures. Energy Procedia 2012;20:217–226.
[2] de Ridder, E., Aalberts, P., van den Berg, J., Buchner, B., Peeringa, J.. The dynamic response of an offshore wind turbine with realistic flexibility to breaking wave impact. In: Proceedings of 30-th International Conference on Offshore Mechanics and Arctic Engineering. 2011,.
[3] Bredmose, H., Jacobsen, N.G.. Breaking wave impacts on offshore wind turbine foundations: Focused wave groups and CFD. In: Proceedings of the 29-th International Conference on Ocean, Offshore and Arctic Engineering. 2010, p. 397–404.
[4] Schløer, S., Bredmose, H., Bingham, H.B., Larsen, T.J.. Effects from fully nonlinear irregular wave forcing on the fatigue life of an offshore wind turbine and its monopile foundation. In: Proceedings of 31-th International Conference on Offshore Mechanics and Arctic Engineering. 2012,.
[5] Cokelet, E.. Breaking waves. Nature 1977;267:769–774.
[6] Goda, Y., Haranaka, S., Kitahata, M.. Study of impulsive breaking wave forces on piles. Tech. Rep.; Port and Harbor Research Institute, Ministry of Transport; 1966.
[7] Kje1dsen, S., Myrhaug, D.. Breaking waves in deep water and resulting wave forces. In: 11th offshore technology conference. 1979, p. 2515–2522.
[8] Chan, E.S.. Mechanics of deep water plunging-wave impacts on vertical structures. Coast Eng 1994;22:115–133.
[9] Sawaragi, T., Nochino, M.. Impact forces of nearly breaking waves on a vertical circular cylinder. Coastal Engineering Journal 1984;27:249–263.
[10] Chaplin, J., Flintham, T., Greated, C., Skyner, D.. Breaking wave forces on a vertical cylinder. Tech. Rep.; Health and Safety Executive,

London, UK; 1992.
[11] Wienke, J., Oumeraci, H.. Breaking wave impact force on a vertical and inclined slender pile-theoretical and large-scale model investigations. Coast Eng 2005;52:435–416.
[12] Arntsen, Ø.A., Ros, X., Tørum, A.. Impact forces on a vertical pile from plunging breaking waves. In: Proceedings of the 24-th Conference on Coastal structures. 2011,.
[13] Morison, J.R., Johnson, J.W., Schaaf, S.A.. The force exerted by surface waves on piles. J Petrol Technol 1950;2:149–154.
[14] Lin, P., Liu, P.L.F.. A numerical study of breaking waves in the surf zone. J Fluid Mech 1998;359:239–264.
[15] Zhao, Q., Armfield, S., Tanimoto, K.. Numerical simulation of breaking waves by a multi-scale turbulence model. Coast Eng 2004;51(1):53–80.
[16] Hieu, P.D., Katsutoshi, T., Ca, V.T.. Numerical simulation of breaking waves using a two-phase flow model. Appl Math Model 2004;28(11):983–1005.
[17] Alagan Chella, M., Bihs, H., Myrhaug, D., Muskulus, M.. Breaking characteristics and geometric properties of spilling breakers over slopes. Coast Eng 2015a;95:4–19.
[18] Alagan Chella, M., Bihs, H., Myrhaug, D.. Characteristics and profile asymmetry properties of waves breaking over an impermeable submerged reef. Coast Eng 2015b;100:26–36.
[19] Alagan Chella, M., Bihs, H., Myrhaug, D., Muskulus, M.. Hydrodynamic characteristics and geometric properties of plunging and spilling breakers over impermeable slopes. Ocean Modelling 2015c;103:53–72.
[20] Mo, W., Jensen, A., Liu, P.L.F.. Plunging solitary wave and its interaction with a slender cylinder on a sloping beach. Ocean Eng 2013;74:48–60.
[21] Choi, S., Lee, K., Gudmestad, O.. The effect of dynamic amplification due to a structures vibration on breaking wave impact. Ocean Eng 2015;96:8–20.
[22] Kamath, A., Alagan Chella, M., Bihs, H., Arntsen, Ø.A.. CFD investigations of wave interaction with a pair of large tandem cylinders. Ocean Eng 2015;108:734–748.
[23] Kamath, A., Bihs, H., Alagan Chella, M., Arntsen, Ø.A.. Upstream-cylinder and downstream-cylinder influence on the hydrodynamics of a four-cylinder group. J Waterw Port Coast Ocean Eng 2016;DOI: 10.1061/(ASCE)WW.1943-5460.0000339.
[24] Alagan Chella, M., Bihs, H., Myrhaug, D., Muskulus, M.. Breaking solitary waves and breaking wave forces on a vertically mounted slender cylinder over an impermeable sloping seabed. Journal of Ocean Engineering and Marine Energy 2016;DOI: 10.1007/s40722-016-0055-5.
[25] Bihs, H., Kamath, A., Alagan Chella, M., Arntsen, Ø.A.. Breaking wave interaction with tandem cylinders under different impact scenarios. J Waterw Port Coast Ocean Eng 2016;DOI: 10.1061/(ASCE)WW.1943-5460.0000343.
[26] Jiang, G.S., Shu, C.W.. Efficient implementation of weighted ENO schemes. J Comput Phys 1996;126:202–228.
[27] Shu, C.W., Osher, S.. Efficient implementation of essentially non-oscillatory shock capturing schemes. J Comput Phys 1988;77:439–471.
[28] Griebel, M., Dornseifer, T., Neunhoeffer, T.. Numerical Simulation in Fluid Dynamics, a Practical Introduction. SIAM; 1998.
[29] Sussman, M., Smereka, P., Osher, S.. A level set approach for computing solutions to incompressible two-phase flow. J Comput Phys 1994;114:146–159.
[30] Peng, D., Merriman, B., Osher, S., Zhao, H., Kang, M.. A PDE-based fast local level set method. J Comput Phys 1999;155:410–438.
[31] Larsen, J., Dancy, H.. Open boundaries in short wave simulations - a new approach. Coast Eng 1983;7:285–297.
[32] Jacobsen, N.G., Fuhrman, D.R., Fredsøe, J.. A wave generation toolbox for the open-source CFD library : OpenFoam. Int J Numer Methods Fluids 2012;70(November):1073–1088.
[33] Schäffer, H.A., Klopman, G.. Review of multidirectional active wave absorption methods. J Waterw Port Coast Ocean Eng 2000;126:88–97.
[34] Berthelsen, P.A., Faltinsen, O.M.. A local directional ghost cell approach for incompressible viscous flow problems with irregular boundaries. J Comput Phys 2008;227:4354–4397.
[35] NOTUR, . The Norwegian Metacenter for Computational Science. http://wwwnoturno/hardware/vilje 2015;.
[36] Fenton, J.. A fifth-order stokes theory for steady waves. J Waterw Port Coast Ocean Eng 1985;111(2):216–234.